*J Mater Sci: Mater Electron* (2021) 32:22760–22770

# Enriched energy storage capability and bi-functional ability of boron-doped graphene as efficient electrode for supercapacitors and lithium sulfur batteries

P. Rajkumar[1], K. Diwakar[1], M. Ramachandran[1,2], A. Mozaffar[3], R. M. Gnanamuthu[4], R. Subadevi[1,*], and M. Sivakumar[1,*]

[1] #120, Energy Materials Lab, Department of Physics, Science Block, Alagappa University, Karaikudi, Tamil Nadu 630003, India
[2] Department of Physics, Arumugam Pillai Seethai Ammal College, Tiruppattur, Tamil Nadu 630211, India
[3] Institute for Particle Technology and Battery LabFactory Braunschweig (BLB), Technische Universität Braunschweig, Volkmaroder Str. 5, 38104 Braunschweig, Germany
[4] Department of Chemistry & Research Institute, SRM Institute of Science and Technology, Kattankulathur, Tamil Nadu 603203, India

**Received:** 19 March 2021
**Accepted:** 16 July 2021
**Published online:** 23 August 2021

© The Author(s), under exclusive licence to Springer Science+Business Media, LLC, part of Springer Nature 2021

## ABSTRACT

This work depicts the preparation of boron-doped graphene (BG) and its application as bi-functional electrode material for both the supercapacitors and lithium–sulfur (Li–S) battery. Structural, morphological, and elemental analyses of the prepared material were acquired via X-ray diffraction, Fourier transform infrared spectroscopy, Raman spectroscopy, Scanning electron microscopy, and X-ray photoelectron spectroscopy, respectively. BG worked well in supercapacitors as a capacitive electrode, featuring a high specific capacitance of 239 F $g^{-1}$ at a current rate of 1 A $g^{-1}$ and high capacity retention of 85% over 10,000 charge/discharge cycles with average coulombic efficiency of 99.5%. In addition, the sulfur/boron-doped graphene (SBG) binary composite was prepared via melt diffusion method and used as the positive electrode material in Li–S batteries. BG is effective polysulfide adsorbent and its sheet-like structure accommodates more content of sulfur, which restricts the shuttle effect and volume changes of active material during cycling. The SBG composite shows an initial discharge capacity of 1355 mAh $g^{-1}$, and it retains the discharge capacity of 636 mAh $g^{-1}$ over the 50 cycles. The present work demonstrates that BG is an efficient electrode material for energy storage applications.

Address correspondence to E-mail: susimsk@yahoo.co.in; susiva73@yahoo.co.in


https://doi.org/10.1007/s10854-021-06650-7

## 1 Introduction

The evolution of mankind in the last decades has seen depletion of the fossil fuels as there is intensification in the consumption of energy globally. The escalation in the risk of climate change, air pollution, and global warming calls for profiteering sustainable energy sources [1, 2]. Thus, mankind is in need of high capacity stable energy storage systems. Supercapacitors and lithium–sulfur (Li–S) batteries are potential energy storage devices, with wide range of application [3–5]. However, both these systems have their pros or cons which require further modification in electrode material.

Attributable to its excellent cycling stability, high power density, and fast charge/discharge ability, supercapacitors are an outstanding way to store energy and favor sustainable development [6–8]. Electric double-layer capacitor (EDLC) and faradic/pseudo-capacitor are two classifications based on their charge storage mechanism. Since they EDLC mechanism involves only surface of electrode materials, they can store low energy density ($< 10$ Wh $kg^{-1}$) and can deliver a very high power density (above 10 kW $kg^{-1}$). Even though batteries exhibit high energy density, they have lower power density compared to supercapacitors [9, 10]. Considering the implicit virtue of high theoretical specific capacity (1675 mAh $g^{-1}$), high energy density (2600 Wh $kg^{-1}$), its ampleness in nature, and non-toxicity of sulfur, lithium–sulfur batteries (LSBs) are currently gratifying substitute for lithium-ion batteries [11–15]. Withal, the challenges like dissolution and shuttling of lithium polysulfides (LPSs), insulating nature of sulfur and lithium sulfides, and lower stability of Li metal anodes hinder the practical implementation of LSBs [16–20]. Hence, it is inevitable to improve the conversion kinetics of polysulfides.

High electronic conductivity, electrolyte ion accessibility, excellent mechanical durability, and commendable chemical stability favor the usage of activated carbon, graphite, graphene, and carbon nanotubes in energy storage systems [21]. Porous carbon materials jointly aid the electrochemical reactions of supercapacitors and batteries, since they shorten ion diffusion path and buffer charge/discharge volume charge. Graphene appealed the researchers' interest with mechanical and chemical stability, high electrical conductivity, and larger specific surface area [22]. On employing pristine graphene as electrode material in energy storage devices like supercapacitors, its performance is afflicted with less specific capacitance. Hence, it is necessary to optimize the oxygen-containing surface functionalities and morphological properties through surface modification in order to improve electrochemical performance of the material [23]. It is seen that carbon materials depicted improved electrical and surface properties and also electrochemical performance of the material is enhanced on introducing sulfur (S), nitrogen (N), boron (B) and phosphorus (P)—heteroatoms [24–27]. Recently electrochemical analyses of doped graphene with several heteroatom dopants such as N, S, P, and B have been reported [28]. By doping on graphene material, it can proficiently alter their electronic structure and intrinsic properties, and affecting the chemical reactions at interfaces, ensuing improved electrochemical performance of the material [29]. Theoretical investigation displays the prospect of lowermost potential barrier for lithium diffusion on B-doped graphene compared to other doped graphene [30, 31]. For Li–S batteries and supercapacitors, boron-doped carbon is an assuring electrode material which improves the conductivity and also the presence of pores enwraps the elemental sulfur. Moreover, when compared to N-, S, and P-doped graphene, the B-doped graphene has lower electronegativity which restrict the shuttle effect of polysulfides and enhance the performance of LSBs. Also, B-doped graphene has high conductivity, creates more number of active sites and good mechanical strength, resulting in improved capacity and better cyclability in a LSB cathode [29, 32, 33]. Apart from this, the interaction of polysulfides with oxygen functional group of graphene results in diffusion of polysulfide; this can be prevented by using boron-doped carbon as electrode material. Supercapacitor conjoined with batteries is an outstanding and viable solution to provide power peaks for starting, accelerating, and stopping electric vehicle.

In this work, boron-doped graphene has been prepared and used for battery and supercapacitor applications. Owing to the property like large surface area and layered structure, graphene can easily accommodate the sulfur particles and thereby reduce the volume expansion. The properties of B-doped sites are expected to be altered due to the low electronegative property of boron [34]. The active sites, thus, created have affinity towards polysulfides and,

hence, alleviate shuttle effect. This work demonstrates boron-doped graphene can be a promising electrode material, providing a high specific capacitance when used in supercapacitors and sulfur composite in Li–S battery for energy storage and conversions.

## 2 Experimental procedure

### 2.1 Preparation of B-doped graphene

For the preparation of boron-doped graphene (BG), 1 g of GO and 0.5 g of boric acid ($H_3BO_3$) were subjected to grinding for about 30 min and were transferred to quartz boat for heat treatment. The boat was placed at midst of parallel quartz cylinder inside a high-temperature furnace. The temperature was set to 500 °C for 1 h and further raised to 700 °C for 1 h at an increasing rate of 3 °C/m in argon atmosphere. Further, the sample was allowed to cool until it reached room temperature to obtain BG. Boron atoms get doped into the vacancies created by the removal of oxygen groups or defects in the structure of graphene.

### 2.2 Preparation of sulfur/BG (SBG) composite

The SBG composite was prepared by melt diffusion method. Initially, 70 wt% of elemental sulfur and 30 wt% of boron-doped graphene were taken and manually mixed for 1 h using mortar and pestle. Then the mixture was shifted to crucible and heat treated at 155 °C for 20 h under argon atmosphere. The sample was then cooled down to room temperature to obtain the final product.

### 2.3 Materials characterization

X-ray diffraction (PANalytical XPERT-PRO with Cu Kα radiation), Fourier transform infrared spectroscopy (Thermo Nicolet 380 Instrumentation Corporation and KBr Pellets), and Raman spectroscopy (STR Raman spectrophotometer, SEKI focal (Japan)) techniques were used for analysis of structural and functional group vibration of the prepared binary composites. The surface morphology of the prepared composites was determined by scanning electron microscopy (ZEISS). X-ray photoelectron spectroscopy (XPS, Theta Probe AR-XPS system) was performed to analyze the chemical composition of the prepared samples.

### 2.4 Electrode preparation and electrochemical measurements

The supercapacitive performance of the BG electrode was evaluated in three-electrode system at room temperature using electrochemical workstation (Bio-Logic instrument SP-300). For the electrode preparation, active material (BG), super P a conductive additive, and PVdF as binder are taken in the weight ratio of 80:10:10 and mixed with N-methyl-2-pyrrolidone (NMP) solvent to form homogeneous slurry. Then the slurry was coated on Ni foam and dried at 80 °C under vacuum. The coated sample was used as working electrode, and Pt and Ag/AgCl as counter and reference electrode. 2 M KOH solution was used as an electrolyte. The cyclic voltammetry (CV) and galvanostatic charge/discharge (GCD) analysis were taken in the potential range of 0–1.0 V.

The coin-type cells (2032) were fabricated in an Ar-filled glove box, using lithium metal as anode, polypropylene sheet as separator, and 1 M lithium bistrifluoromethanesulfonyl imide (LiTFSI) containing 0.05 M $LiNO_3$ in 1,2-dimethoxyethane/1,3-dioxolane (1:1, V/V) as electrolyte for Li–S battery. Active material (SBG composite), super P, and polyvinylidene fluoride (PVDF) in N-methyl-2-pyrrolidone (NMP) solvent with a weight ratio of 7:2:1 were pulverized to form slurry and was coated on aluminum foil which was dried in vacuum oven at 60 °C for 1 day. Thus, procured film was pressed into circular shape with 12 mm diameter, which is used as positive working electrode. Cyclic voltammetry and galvanostatic charge/discharge tests were carried out within a voltage range of 1.5–3.0 V using biologic (BCS 815, France) battery tester.

## 3 Results and discussion

Phase structures of the BG and SBG composite were examined using X-ray diffraction (XRD) technique. XRD patterns of the pure sulfur, boron-doped graphene and SBG composite are depicted in Fig. 1a. In Fig. 1a, the pure sulfur diffraction peaks show standard sequence of orthorhombic sulfur (JCPDS No. 08-0247) with space group of Fddd. The GO

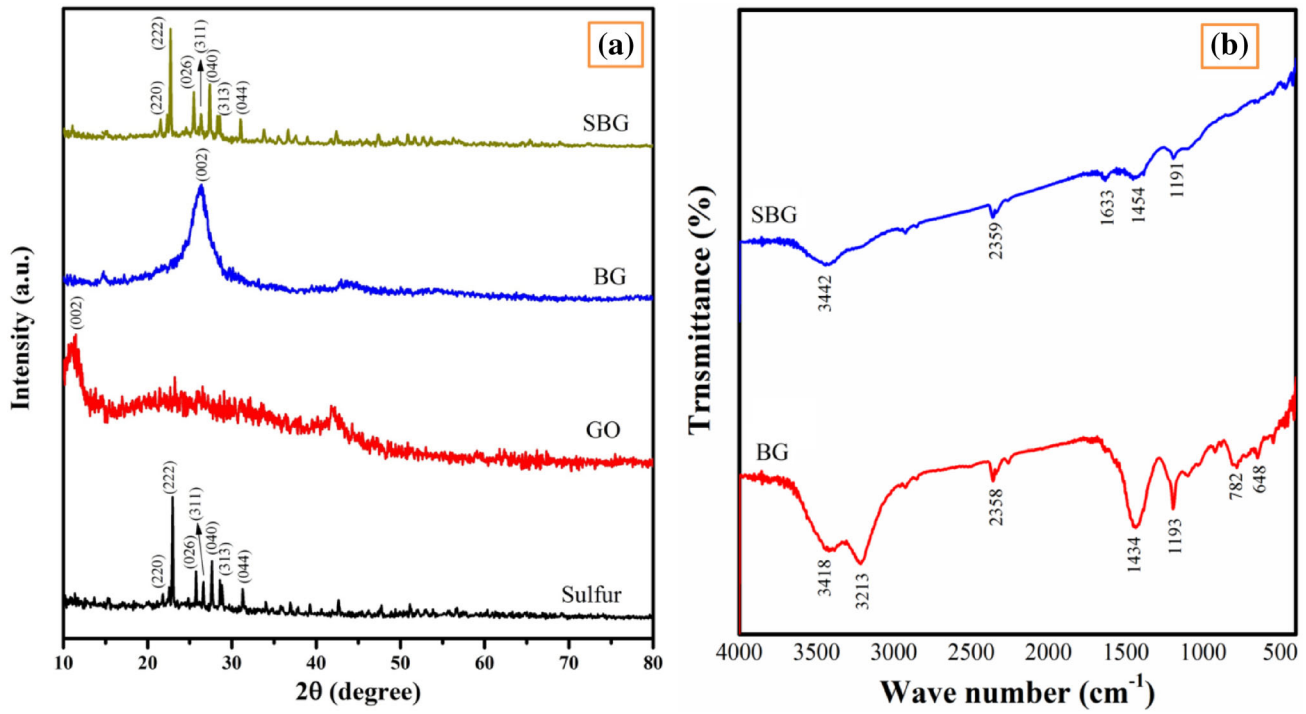


**Fig. 1** **a** XRD patterns of pure sulfur, boron-doped graphene, SBG composite; **b** FTIR spectra of the as-prepared BG and SBG composite

diffraction peak (Fig. 1b) was centered at $2\theta = 11°$, corresponds to the typical (002) plane and originated owing to oxygen functionalities. After heat treatment, the GO peak entirely deduced due to the deoxidization of GO, whereas the BG (Fig. 1c) exhibits broad peak at $2\theta = 25°$ which corresponds to the (002) plane. The diffraction pattern of SBG composite is concurrent with that of sulfur as shown in Fig. 1a. The functional group vibrations of the prepared SBG composite were determined using Fourier Transform Infrared Spectroscopy (FTIR). Figure 1b shows the FTIR spectra in the range of 4000–400 $cm^{-1}$. The boron-doped graphene and SBG composite show broad and intense peak in the range 3400–3100 $cm^{-1}$ representing the O–H stretching vibration. The peak located at 782 $cm^{-1}$ as seen in FTIR spectra of BG belongs to the vibration of epoxy groups. The peak at 648 $cm^{-1}$ can be assigned to the O–B–O bond [35]. The asymmetric vibration of C–H is the reason for the presence of infrared bands at 1454 and 1434 $cm^{-1}$, and the symmetric C–H vibration can be ascribed to the presence of peak around 1190 $cm^{-1}$. The band at 1633 $cm^{-1}$ and 2359 $cm^{-1}$ can be attributed to the bending vibration of O–H and existence of atmospheric $CO_2$ [13].

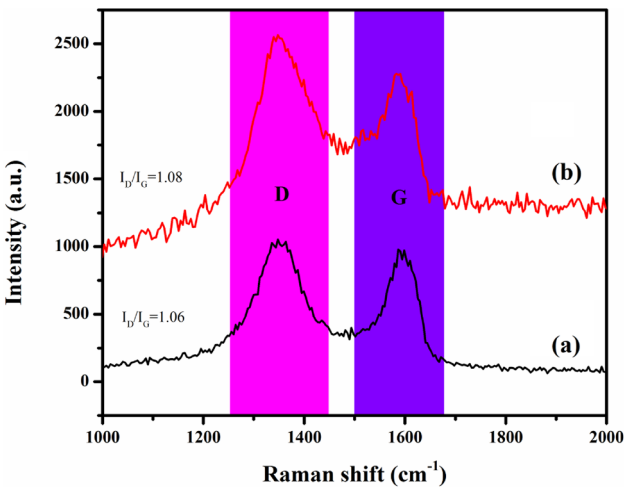


**Fig. 2** Raman spectra of the as-prepared (*a*) BG and (*b*) SBG composite

Figure 2 shows the Raman spectra of the prepared BG and SBG composites. Both the spectra exhibit two well-known D and G bands. The D band observed at 1345 $cm^{-1}$ denoting the disorderliness in the structure of BG. The G band at 1583 $cm^{-1}$ is the characteristic peak associated with the graphitic structure of BG [36, 37]. The intensity ratio is calculated to be ($I_D$/$I_G$) of 1.06 for BG and 1.08 for SBG, which indicates the presence of more defects on the prepared

composite [38]. The presence of carbon in the prepared SBG composite is evident from the above results. The surface morphology of the prepared samples were analyzed using scanning electron microscopy. In Fig. 3a, b, crumpled sheets of BG sample can be seen, before the addition of sulfur. After sulfur infusion into BG (Fig. 3c, d), the same wrinkled structured could be observed. It confirms that the layered structure of BG sheets easily accommodates the sulfur particles, which may restrict the volume expansion of active material during cycling process.

The chemical composition of prepared samples are analyzed using XPS technique. Figure 4a illustrates the survey spectra of SBG. The existence of B1s, S2p, and S2s peaks in SBG composite indicates effective doping of boron and sulfur combination in the as-prepared sample. The survey spectrum shows C1s and O1s peaks at 284.0 and 531.0 eV, respectively. The deconvoluted B1s spectra (Fig. 4b) exhibited peaks at 191.2 and 192.6 eV which can be attributed to the presence of $-BC_3$, $-BC_2O$, and $-BCO_2$ bonds [39, 40], signifying boron atoms are attached to the carbon matrix. The high-resolution S2p spectra (Fig. 4c) display two main peaks of $S2p_{3/2}$ and $S2p_{1/2}$ at 163.9 and 165.1 eV, which indicates the presence of C–S bonds in the composite [41]. From Fig. 4d, the C1s spectra display 3 distinct peaks at 288.5, 285.9, and 284.7 eV, which corresponding to the carbon bonds in graphene structure with different chemical environments. The narrow peak at 287.7 eV corresponds to the C–C $sp^2$-bonded graphite like carbon, suggesting that the most of carbon atoms are agreed in a conjugated honeycomb structure in the composite [31]. From the XPS spectra, it is evident that the amalgamation of heteroatom (B) into the SBG structure.

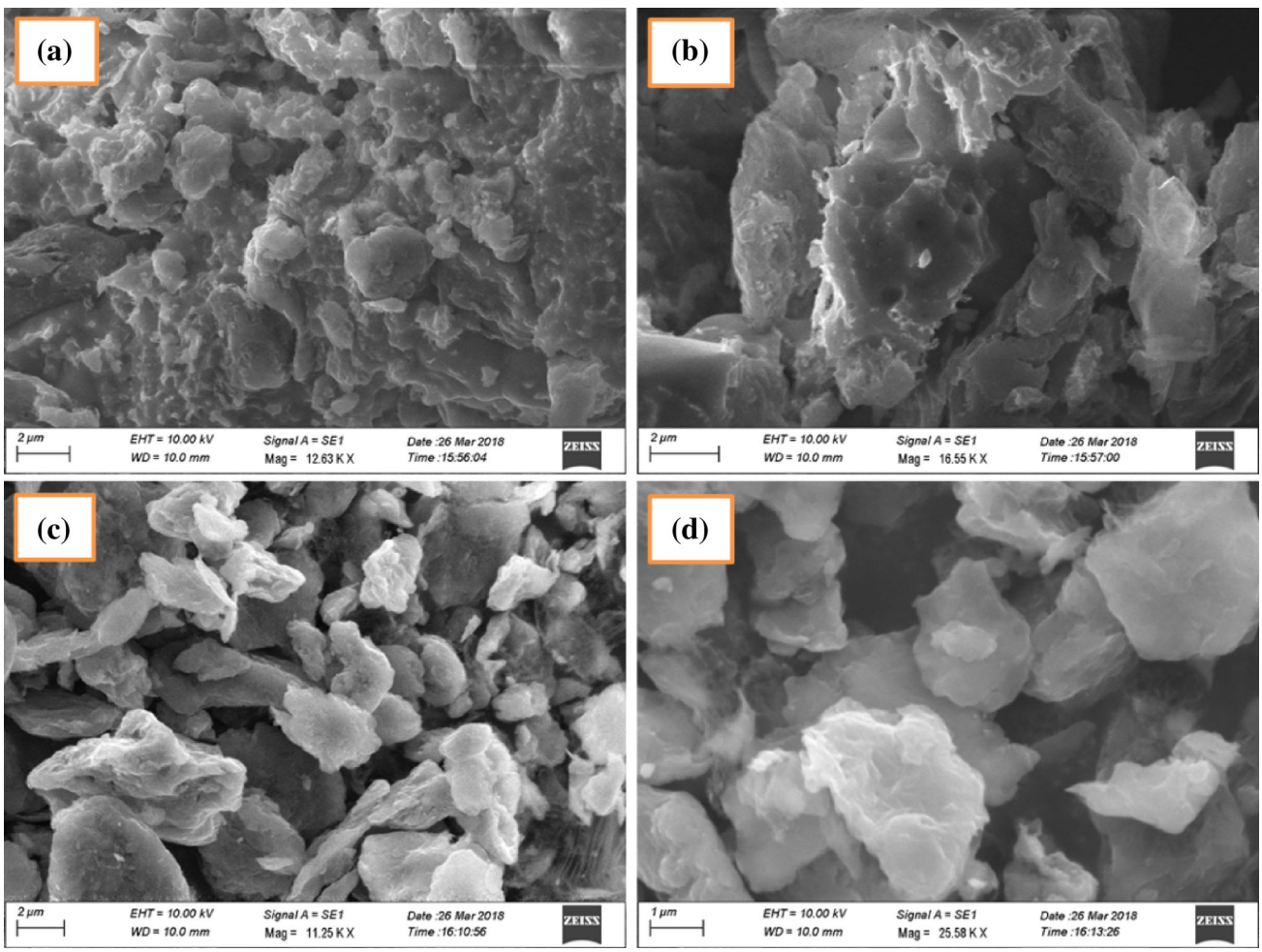


**Fig. 3** SEM images of (**a**, **b**) B-doped graphene; (**c**, **d**) SBG composite

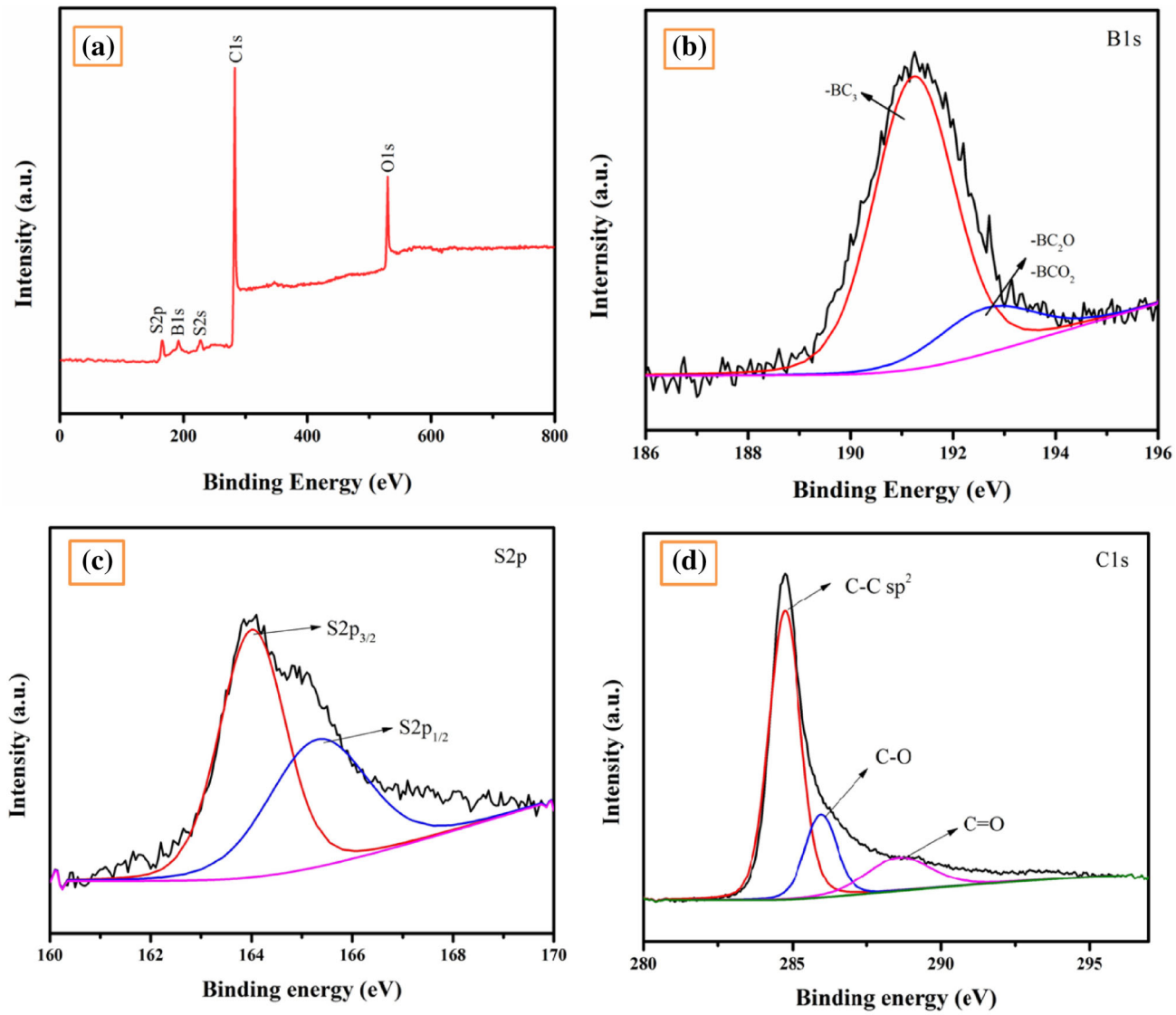


**Fig. 4** **a** XPS survey spectrum of SBG composite and deconvoluted spectra of **b** B1s, **c** S2p, and **d** C1s

## 3.1 Supercapacitive performance

In this study, BG sample is tested as electrode material for supercapacitor. The fabrication of electrode is described in experimental section. The Cyclic Voltammetry curve of BG electrode is shown in Fig. 5a. The curves are recorded in the following series of scan rate 10, 20, 40, 60, 80, and 100 mV/s. The capacitance is obtained within the voltage window of − 1.0 to 0 V. A decrease in capacitance is observed as scan rate is increased, which is due to the declination in the ions diffusing into the electrode surface. As the scan rate is increased from 10 to 100 mV/s, the capacitance is seen to decrease from 270 to 130 F $g^{-1}$. Galvanostatic charge discharge (GCD) curve is obtained for the current densities 1, 2, 3, 5, and 10 A/g. The triangular shape of GCD curve (Fig. 5b) indicates pseudo-capacitive behavior of supercapacitor with BG electrode. The capacitance varies from 239 to 152 F $g^{-1}$ as current density is varied from 1 to 10 A/g. The BG electrode delivers an outstanding capacitance and columbic efficiency around 85 and 99.5% after 10,000 cycles as shown in Fig. 5c. High capacitance with good cyclic stability proves that BG is a potential electrode material for supercapacitors.

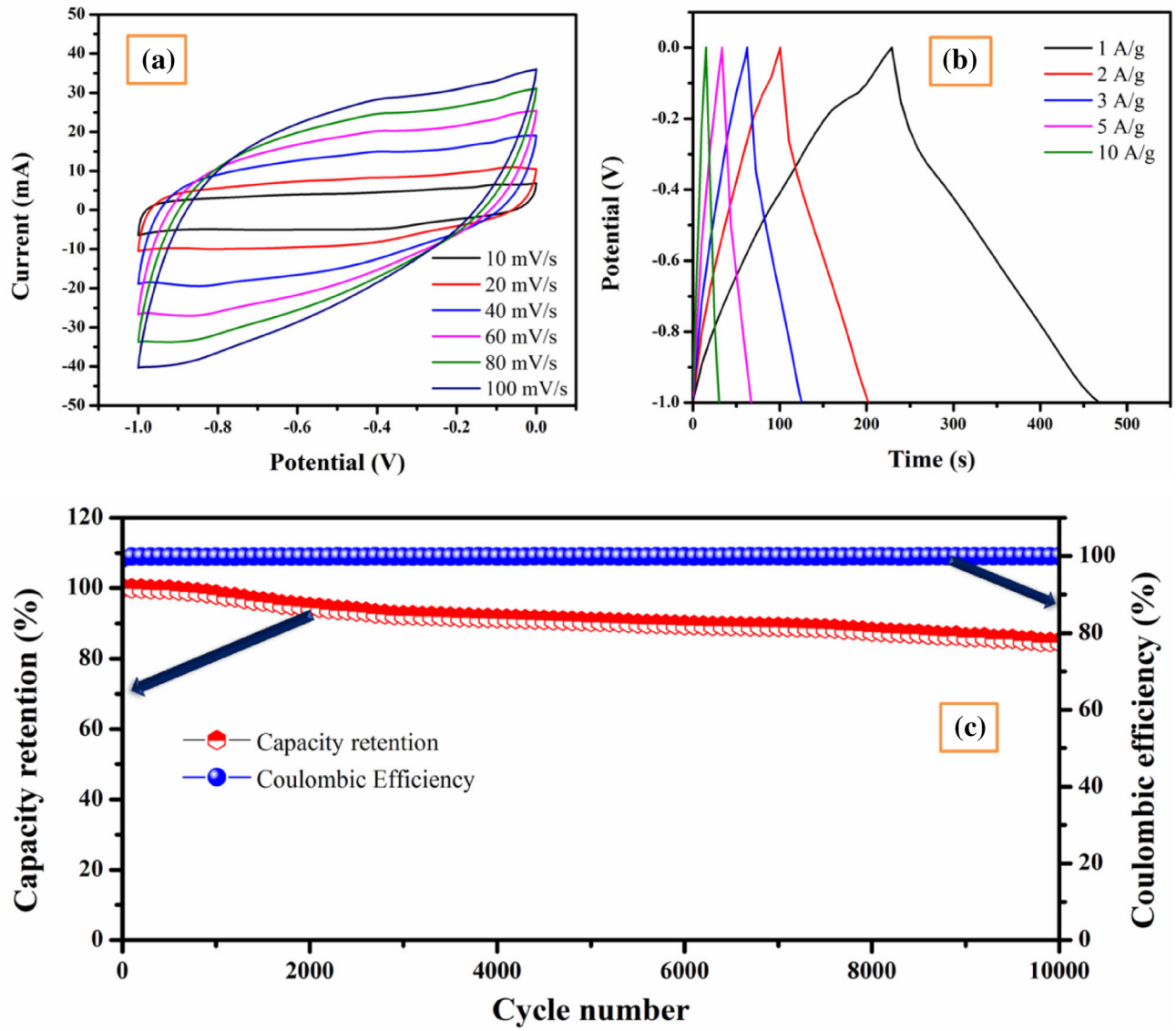


**Fig. 5** Electrochemical performance of BG electrode in supercapacitor: **a** cyclic voltammetry, **b** Charge/discharge profile at various rates, and **c** capacity retention and coulombic efficiency at 5 A $g^{-1}$ over 10,000 cycles

## 3.2 Li–S battery performance

The electrochemical performance of the SBG binary composite cathode for Li–S battery was further examined. Figure 6a depicts the initial 2-cycle cyclic voltammetry (CV) curves of the prepared cathode at a scan rate of 0.1 mV $s^{-1}$ with the potential range of 1.5–3.0 V. During cathodic scan, two reduction peaks associated to reduction reaction of sulfur can be observed. The peak at 2.22 V corresponds to the transformation of elemental sulfur to higher-order lithium polysulfides ($Li_2S_n$, $4 \leq n < 8$) and the peak at 1.97 V further transformation of higher-order to lower-order lithium polysulfides ($Li_2S_2$ or $Li_2S$) [42, 43]. During anodic scan, only one oxidation peak is observed at 2.5 V ascribed to the conversion of lower-order polysulfides to elemental sulfur. After the initial cycle, the second cycle CV curves of peak currents, voltage potentials, and peak areas are almost overlapped, which indicating that the SBG composite has better reversibility. Figure 6b shows the galvanostatic charge/discharge profile of the prepared binary composite in the current rate of 0.1 C. From the charge/discharge profile, two well-known reduction peaks and one oxidation peak was observed, which is consistent with the CV curves (Fig. 6a). The prepared SBG binary composite

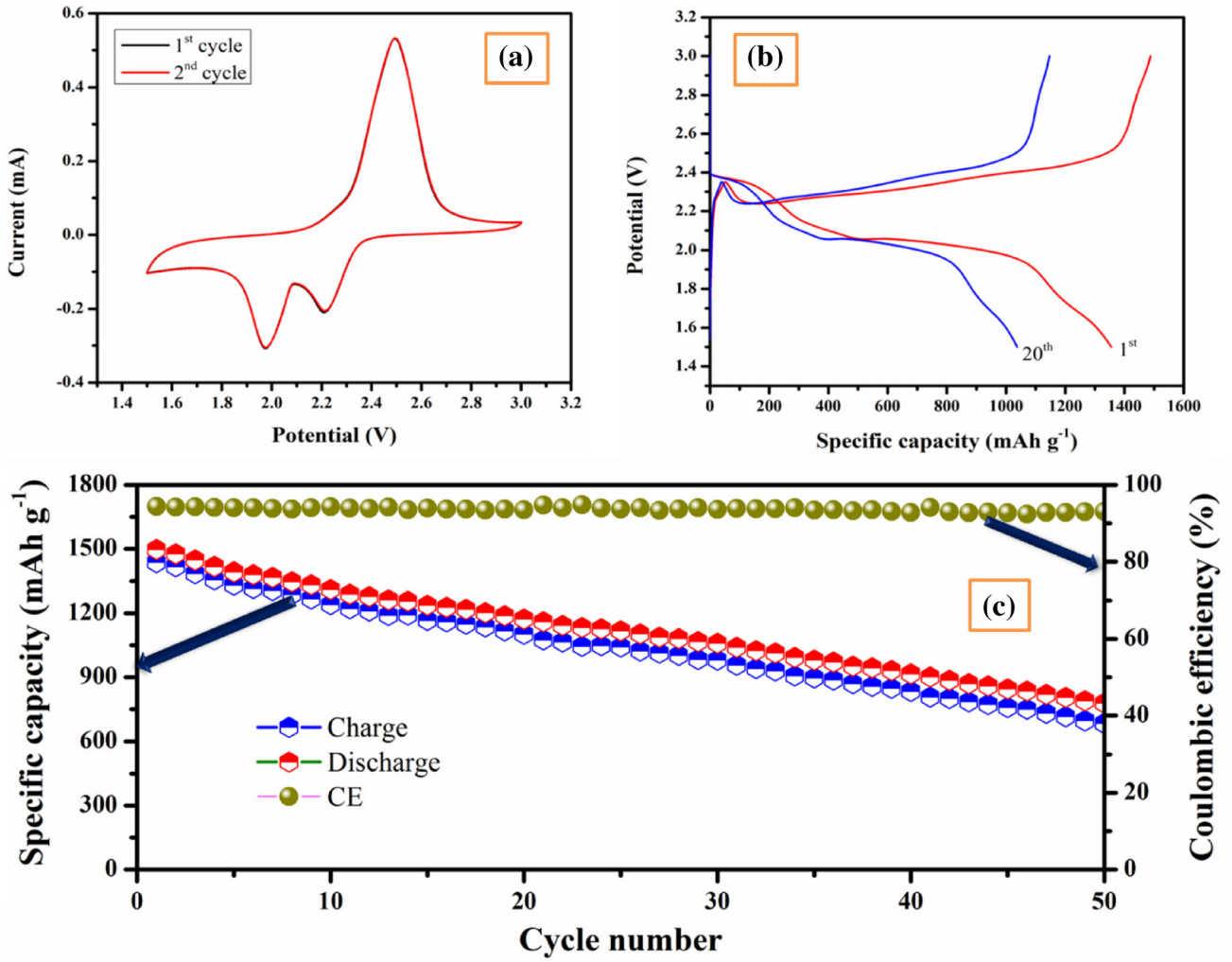


**Fig. 6** Electrochemical performance of SBG composite cathode in Li–S battery: **a** cyclic voltammetry, **b** Charge/discharge profile at 0.1 C rate, and **c** cycling performance and coulombic efficiency at 0.1 C

cathode exhibits discharge capacities of 1355 and 1102 mAh $g^{-1}$ for initial and 20th cycle, respectively. From Fig. 6c, the SBG cathode maintains the discharge capacity of 636 mAh $g^{-1}$ with the average coulombic efficiency of 90% over the 50th cycle. The high initial discharge capacity of SBG cathode demonstrates that the B-doping provides effective conduction pathway in the sulfur electrode and the utilization of active material is high. Moreover, the doped B atoms can create more number of active sites, as a result, which offered distinct ability to chemical adsorption and alleviate polysulfides [39].

Further the SBG cathode was examined by rate capability investigation with various current densities from 0.1 to 1 C as shown in Fig. 7. The composite cathode exhibits a discharge capacity of 1355, 975, 644, and 418 mAh $g^{-1}$ at the current densities of 0.1,

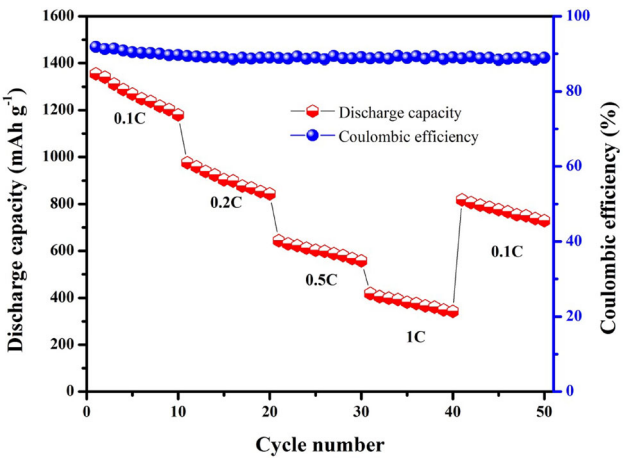


**Fig. 7** Discharge capacities of SBG at varying rates from 0.1 C to 1 C

**Table 1** Performance of prepared SBG composite cathode compared with previously reported carbon-based sulfur cathodes

| Electrode material | Current density | Initial discharge capacity (mAh $g^{-1}$) | References |
|---|---|---|---|
| S/GA | 0.1 C | 1100 | [44] |
| S-prGO | 0.1 C | 893 | [42] |
| AC/S | 0.05 C | 1120 | [45] |
| S@C | 0.1 C | 1305 | [46] |
| S-AB | 40 mA/g | 934 | [47] |
| SNG | 0.1 C | 1135 | [48] |
| SBG | 0.1 C | 1355 | This work |

0.2, 0.5, and 1 C, respectively. When the current density was swapped to 0.2 C rate, the SBG cathode maintains a discharge capacity of 818 mAh $g^{-1}$, which demonstrating that the structure of SBG cathode remains stable even at high rates. The better performance of BG, due to the positively polarized B atoms, adsorbs the negative polysulfides which deteriorates shuttle effect and enhances stability of BG electrode. Moreover, while comparing the earlier reported carbon-based sulfur composites, the SBG composite exhibits better initial discharge capacity [42, 44–48], as exposed in Table 1. From the electrochemical performances of supercapacitors and L-S battery, the boron-doped graphene was promising electrode for energy storage applications.

## 4 Conclusion

Concisely, boron-doped graphene was successfully prepared and applied as progressive electrodes for supercapacitors and efficient sulfur host for Li–S battery cathode. BG deployed as an electrode in supercapacitor gave high capacitance of 239 F $g^{-1}$ at 1 A $g^{-1}$ and high cyclic stability with enhanced coulombic efficiency. Moreover, the prepared BG adopted as sulfur host in cathode material of Li–S battery, it exhibited the high initial discharge capacity of 1355 mAh $g^{-1}$ at 0.1 C. The adsorption capability of BG with polysulfides effectively alleviates the active material loss and shuttle effect, and the layered structure of graphene sheets restricts the volume expansion of active material during cycling process. These results show that boron-doped graphene as efficient electrode material for energy storage applications.

## Acknowledgements

All the authors from Alagappa University acknowledge the financial support by DST-SERB, New Delhi under the Physical sciences, grant sanctioned vide EMR/2016/006302. Also, all the authors gratefully acknowledge for extending the analytical facilities in the Department of Physics, Alagappa University under the PURSE and FIST programme, sponsored by Department of Science and Technology (DST), Special Assistance Programme (SAP) sponsored by University Grants Commission (UGC), New Delhi, Govt. of India and Ministry of Human Resource Development RUSA- Phase 2.0 grant sanctioned vide Lt.No.F-24-51/2014 U Policy (TNMulti Gen), Dept. of Education, Govt. of India.

## References

1. D.J. Tarimo, K.O. Oyedotun, A.A. Mirghni, N.F. Sylla, N. Manyala, Electrochim. Acta **353**, 136498 (2020). https://doi.org/10.1016/j.electacta.2020.136498
2. G. Babu, A. Sawas, N.K. Thangavel, L.M.R. Arava, J. Phys. Chem. C **122**(20), 10765–10772 (2018). https://doi.org/10.1021/acs.jpcc.8b02633
3. Y. Zhang, Z. Gao, N. Song, X. Li, Electrochim. Acta **222**, 1257–1266 (2016). https://doi.org/10.1016/j.electacta.2016.11.099
4. J. Cai, Y. Song, X. Chen, Z. Sun, Y. Yi, J. Sun, Q. Zhang, J. Mater. Chem. A **8**(4), 1757–1766 (2020). https://doi.org/10.1039/C9TA11958B
5. P. Rajkumar, K. Diwakar, G. Radhika, K. Krishnaveni, R. Subadevi, M. Sivakumar, Vacuum **161**, 37–48 (2019). https://doi.org/10.1016/j.vacuum.2018.12.016
6. M. Abdollahifar, H.W. Liu, C.H. Lin, Y.T. Weng, H.S. Sheu, J.F. Lee, M.L. Lu, Y.F. Liao, N.L. Wu, Energy Environ. Mater. **3**(3), 405–413 (2020). https://doi.org/10.1002/eem2.12094

7. D. Karuppiah, R. Palanisamy, A. Ponnaiah, S. Rengapillai, S. Marimuthu, Int. J. Energy Res. **44**(9), 7591–7602 (2020). https://doi.org/10.1002/er.5492
8. S. Zang, J. Jiang, Y. An, Z. Li, H. Guo, Y. Sun, H. Dou, X. Zhang, J. Electroanal. Chem. **876**, 114723 (2020). https://doi.org/10.1016/j.jelechem.2020.114723
9. S. Alagar, R. Madhuvilakku, R. Mariappan, S. Piraman, J. Mater. Sci. Mater. Electron. **29**(2), 1173–1181 (2018). https://doi.org/10.1007/s10854-017-8019-7
10. D. Cericola, P. Novák, A. Wokaun, R. Kötz, J. Power Sources **196**(23), 10305–10313 (2011). https://doi.org/10.1016/j.jpowsour.2011.07.032
11. K. Kalaiappan, S. Rengapillai, S. Marimuthu, R. Murugan, P. Thiru, Front. Chem. Sci. Eng. **14**, 976–987 (2020). https://doi.org/10.1007/s11705-019-1897-x
12. N. Zheng, G. Jiang, X. Chen, J. Mao, N. Jiang, Y. Li, Nanomicro Lett. **11**(1), 43 (2019). https://doi.org/10.1007/s40820-019-0275-z
13. P. Rajkumar, K. Diwakar, R. Subadevi, R.M. Gnanamuthu, F.M. Wang, M. Sivakumar, J. Phys. D Appl. Phys. **53**(26), 265501 (2020). https://doi.org/10.1088/1361-6463/ab8137
14. G. Radhika, R. Subadevi, K. Krishnaveni, W.R. Liu, M. Sivakumar, J. Nanosci. Nanotechnol. **18**(1), 127–131 (2018). https://doi.org/10.1166/jnn.2018.14568
15. J. Shi, Q. Kang, Y. Mi, Q. Xiao, Electrochim. Acta **324**, 134849 (2019). https://doi.org/10.1016/j.electacta.2019.134849
16. K. Krishnaveni, R. Subadevi, M. Sivakumar, M. Raja, T. Prem Kumar, J. Sulfur Chem. **40**(4), 377–388 (2019). https://doi.org/10.1080/17415993.2019.1582655
17. Y. Chen, S. Choi, D. Su, X. Gao, G. Wang, Nano Energy **47**, 331–339 (2018). https://doi.org/10.1016/j.nanoen.2018.03.008
18. G. Radhika, K. Krishnaveni, C. Kalaiselvi, R. Subadevi, M. Sivakumar, Polym. Bull. **77**, 4167–4179 (2020). https://doi.org/10.1007/s00289-019-02963-0
19. K. Wu, Y. Hu, Z. Shen, R. Chen, X. He, Z. Cheng, P. Pan, J. Mater. Chem. A **6**(6), 2693–2699 (2018). https://doi.org/10.1039/C7TA09641K
20. K. Kalaiappan, S. Marimuthu, S. Rengapillai, R. Murugan, T. Premkumar, Ionics **25**(10), 4637–4650 (2019). https://doi.org/10.1007/s11581-019-03018-0
21. J.H. Kang, J.S. Chen, Diam. Relat. Mater. **88**, 222–229 (2018). https://doi.org/10.1016/j.diamond.2018.07.015
22. J.Y. Hong, J.J. Wie, Y. Xu, H.S. Park, Phys. Chem. Chem. Phys. **17**(46), 30946–30962 (2015). https://doi.org/10.1039/C5CP04203H
23. T. Tojo, K. Sakurai, H. Muramatsu, T. Hayashi, K.S. Yang, Y.C. Jung, C.M. Yang, M. Endo, Y.A. Kim, RSC Adv. **4**(107), 62678–62683 (2014). https://doi.org/10.1039/C4RA10439K
24. W. Kiciński, M. Szala, M. Bystrzejewski, Carbon **68**, 1–32 (2014). https://doi.org/10.1016/j.carbon.2013.11.004
25. Q. Li, J. Guo, J. Zhao, C. Wang, F. Yan, Nanoscale **11**(2), 647–655 (2019). https://doi.org/10.1039/C8NR07220E
26. C.P. Yang, Y.X. Yin, H. Ye, K.C. Jiang, J. Zhang, Y.G. Guo, A.C.S. Appl, Mater. Interfaces **6**(11), 8789–8795 (2014). https://doi.org/10.1021/am501627f
27. J. Tan, D. Li, Y. Liu, P. Zhang, Z. Qu, Y. Yan, H. Hu, H. Cheng, J. Zhang, M. Dong, C. Wang, J. Mater. Chem. A **8**(16), 7980–7990 (2020). https://doi.org/10.1039/D0TA00284D
28. H. Liu, Y. Liu, D. Zhu, J. Mater. Chem. **21**, 3335–3345 (2011). https://doi.org/10.1039/C0JM02922J
29. R. Kumar, S. Sahoo, E. Joanni, R.K. Singh, K. Maegawa, W.K. Tan, G. Kawamura, K.K. Kar, A. Matsuda, Mater. Today **39**, 47–65 (2020). https://doi.org/10.1016/j.mattod.2020.04.010
30. S. Gao, Z. Ren, L. Wan, J. Zheng, P. Guo, Y. Zhou, Appl. Surf. Sci. **257**, 7443–7446 (2011). https://doi.org/10.1016/j.apsusc.2011.02.135
31. M. Sahoo, K.P. Sreena, B.P. Vinayan, S. Ramaprabhu, Mater. Res. Bull. **61**, 383–390 (2015). https://doi.org/10.1016/j.materresbull.2014.10.049
32. R. Kumar, S. Sahoo, E. Joanni, R.K. Singh, W.K. Tan, K.K. Kar, A. Matsuda, Carbon **177**, 304–331 (2021). https://doi.org/10.1016/j.carbon.2021.02.091
33. R. Kumar, S. Sahoo, E. Joanni, R.K. Singh, W.K. Tan, K.K. Kar, A. Matsuda, Prog. Energy Combust. Sci. **75**, 100786 (2019). https://doi.org/10.1016/j.pecs.2019.100786
34. X. Yu, P. Han, Z. Wei, L. Huang, Z. Gu, S. Peng, J. Ma, G. Zheng, Joule **2**(8), 1610–1622 (2018). https://doi.org/10.1016/j.joule.2018.06.007
35. A.K. Yadav, P. Singh, RSC Adv. **5**(83), 67583–67609 (2015). https://doi.org/10.1039/C5RA13043C
36. K. Mi, S. Chen, B. Xi, S. Kai, Y. Jiang, J. Feng, Y. Qian, S. Xiong, Adv. Func. Mater. **27**(1), 1604265 (2017). https://doi.org/10.1002/adfm.201604265
37. R. Palanisamy, D. Karuppiah, S. Rengapillai, G. Ramasamy, M. Abdollahifar, F.M. Wang, S. Marimuthu, JOM **72**, 2260–2268 (2020). https://doi.org/10.1007/s11837-020-04165-w
38. M. Xiang, Y. Wang, J. Wu, Y. Guo, H. Wu, Y. Zhang, H. Liu, Electrochim. Acta **227**, 7–16 (2017). https://doi.org/10.1016/j.electacta.2016.11.139
39. P. Shi, Y. Wang, X. Liang, Y. Sun, S. Cheng, C. Chen, H. Xiang, A.C.S. Sustain, Chem. Eng. **6**(8), 9661–9670 (2018). https://doi.org/10.1021/acssuschemeng.8b00378
40. Y. Tian, C. Deng, Z. Sun, Y. Zhao, T. Tan, F. Yin, X. Wang, Int. J. Electrochem. Sci. **13**, 3441–3451 (2018). https://doi.org/10.20964/2018.04.37

41. Y. Lu, S. Gu, J. Guo, K. Rui, C. Chen, S. Zhang, J. Jin, J. Yang, Z. Wen, A.C.S. Appl, Mater. Interfaces **9**(17), 14878–14888 (2017). https://doi.org/10.1021/acsami.7b02142
42. P. Rajkumar, K. Diwakar, R. Subadevi, R.M. Gnanamuthu, M. Sivakumar, Curr. Appl. Phys. **19**(8), 902–909 (2019). https://doi.org/10.1016/j.cap.2019.05.001
43. K. Krishnaveni, R. Subadevi, M. Raja, T. PremKumar, M. Sivakumar, J. Appl. Polym. Sci. **135**(34), 46598 (2018). https://doi.org/10.1002/app.46598
44. X.G. Sun, X. Wang, R.T. Mayes, S. Dai, Chemsuschem **5**, 2079–2085 (2012). https://doi.org/10.1002/cssc.201200101
45. Y. Chen, N. Liu, H. Shao, W. Wang, M. Gao, C. Li, H. Zhang, A. Wang, Y. Huang, J. Mater. Chem. A **3**, 15235–15240 (2015). https://doi.org/10.1039/C5TA03032C
46. Y.S. Su, Y. Fu, T. Cochell, A. Manthiram, Nat. Commun. **4**, 2985 (2013). https://doi.org/10.1038/ncomms3985
47. B. Zhang, C. Lai, Z. Zhou, X.P. Gao, Electrochim. Acta **54**, 3708–3713 (2009). https://doi.org/10.1016/j.electacta.2009.01.056
48. P. Rajkumar, K. Diwakar, K. Krishnaveni, G. Radhika, R. Subadevi, R.M. Gnanamuthu, F.-M. Wang, M. Sivakumar, J. Mater. Eng. Perform. **29**, 2865–2870 (2020). https://doi.org/10.1007/s11665-020-04825-7

**Publisher's Note** Springer Nature remains neutral with regard to jurisdictional claims in published maps and institutional affiliations.